Water Resources Research

RESEARCH ARTICLE
10.1029/2025WR040785

Influence of Hydraulic Conductivity Conceptualization and Unsaturated Flow Parameters for an Integrated Hydrological Model

Edinsson Muñoz-Vega[1], Heye Reemt Bogena[2], Juan Carlos Richard-Cerda[1], Reed M. Maxwell[3,4,5], and Stephan Schulz[1]

[1]Technische Universität Darmstadt, Institute of Applied Geosciences, Darmstadt, Germany, [2]Forschungszentrum Jülich GmbH, Institute of Bio- and Geosciences, Agrosphere Institute (IBG-3), Jülich, Germany, [3]Department of Civil and Environmental Engineering, Princeton University, Princeton, NJ, USA, [4]Integrated GroundWater Modeling Center, Princeton University, Princeton, NJ, USA, [5]High Meadows Environmental Institute, Princeton University, Princeton, NJ, USA

Key Points:

- A comprehensive sensitivity analysis was performed to analyze the effects of subsurface parametrization for an integrated hydrologic model
- The magnitude and anisotropy of the hydraulic conductivity of shallow horizons control streamflow behavior
- Soil water retention curve and linked parameters such as field capacity and wilting point regulate moisture distribution during dry periods

Supporting Information:

Supporting Information may be found in the online version of this article.

Correspondence to:

E. Muñoz-Vega,
edinsson.munoz@tu-darmstadt.de

Citation:

Muñoz-Vega, E., Bogena, H. R., Richard-Cerda, J. C., Maxwell, R. M., & Schulz, S. (2025). Influence of hydraulic conductivity conceptualization and unsaturated flow parameters for an integrated hydrological model. *Water Resources Research*, *61*, e2025WR040785. https://doi.org/10.1029/2025WR040785

Received 10 APR 2025
Accepted 27 OCT 2025

Abstract In recent decades, integrated hydrologic models (IHMs) have advanced our understanding of hydrologic processes across catchment to continental scales. These models couple surface and variably saturated subsurface flow, incorporating land surface models to represent interactions within the critical zone. However, high computational costs hinder calibration and sensitivity analysis. Prior studies show that outputs such as runoff, soil moisture, and energy fluxes are highly sensitive to subsurface parametrization, particularly to the hydraulic conductivity (K) in both saturated and unsaturated zones. Despite its relevance in soil-vegetation interactions, sensitivity to unsaturated parameters has been less explored, often limited to synthetic domains. To address this, we designed a deterministic approach consisting of 55 simulations, to explore K and other parameters sensitivities. We employed the parallel, fully integrated model Parflow-CLM to simulate water and energy fluxes in a headwater catchment in the Odenwald, Germany. Simulations were evaluated against streamflow and soil moisture observations to ensure realistic results. Multiple combinations of K-values, anisotropies, and van Genuchten parameters were tested, examining the impact of soil hydraulic properties on plant water uptake. Results show that increasing K enhances baseflow and attenuates peak flows, while anisotropy in shallow horizons significantly affects runoff and groundwater dynamics. The shape of the soil water retention curve, represented by the van Genuchten parameters, as well as saturation at field capacity and wilting point, strongly influence simulated soil moisture during dry periods. Overall, our analysis provides insights into subsurface parameter sensitivities to hydrologic responses, supporting the design of calibration schemes for IHM applications.

1. Introduction

Interactions between surface water and groundwater are fundamental processes of the hydrologic cycle (Kollet & Maxwell, 2006). Over the last decades, the exploration of this interaction has driven the development of integrated hydrologic models (IHMs), which directly link surface and subsurface flow equations. IHMs are often further coupled with land surface models (Kuffour et al., 2020) to provide a comprehensive understanding of the hydrological processes in the critical zone, extending from bedrock to atmosphere (Brooks et al., 2015). Therefore, IHMs typically cover depths of tens to hundreds of meters, highlighting the importance of both the shallow and deep subsurface in catchment hydrology (Condon et al., 2020). However, this also introduces significant complexity due to the inherent challenges associated with the conceptualization and calibration of hydrogeological models (Rojas et al., 2008; Seifert et al., 2012), including the representation of geometry, system boundaries, physical properties, usually under data scarcity (Enemark et al., 2019).

With regard to the physical properties of the subsurface, one of the main factors controlling flow in the vadose zone and groundwater is the hydraulic conductivity (K), which is usually characterized by high degrees of heterogeneity (Sanchez-Vila et al., 2006). K is particularly important for IHMs, because it contributes to the determination of subsurface water flow and its interaction with land surface processes (Lu et al., 2024). Despite its importance, limited research has investigated model sensitivity to K parametrization in real domains (Foster, 2018; Herzog et al., 2021). Theoretical studies, however, have demonstrated that model results in terms of streamflow, groundwater table dynamics (Engdahl, 2024; Rapp et al., 2020), soil moisture distribution (Atchley

& Maxwell, 2011; Leonarduzzi et al., 2021) and energy fluxes (Kollet, 2009) are highly sensitive to K conceptualization. Moreover, K is scale dependent by definition (Sanchez-Vila et al., 2006), and various approaches have been proposed for IHMs to address this issue (Fang et al., 2016; Foster, 2018; Niedda, 2004), including considerations for the loss of topographic information with decreasing numerical grid resolution.

Another critical aspect of K is its anisotropic behavior due to mostly layered heterogeneities that are present in scales from micrometers to kilometers particularly in sedimentary strata (Shepley, 2024). Consequently, full K tensors are required to parametrize natural porous media (Chiogna et al., 2015; Schulz et al., 2017). However, anisotropy has received little attention in the context of IHMs. Rapp et al. (2020), evaluated different scenarios of an idealized headwater catchment, including one anisotropic case with lower vertical K than horizontal K in all the conceptualized hydrogeological units, which resulted in reduced flow path depths and river discharges controlled by storage but with little effects on governing surface runoff. Conversely, Fang et al. (2015) incorporated a higher horizontal K with respect to the vertical K for the soil layer that overlies an impermeable bedrock in a forested catchment to represent interflow processes and could observe important effects on surface runoff and soil moisture dynamics. Although both studies indicate that IHMs are sensitive to K anisotropy, the contrasting results show that further investigations are required to understand the implications of anisotropic K fields for IHMs.

The parametrization of K in IHMs also accounts for its behavior under unsaturated conditions to solve adapted versions of the Richards' equation for variably saturated flow (Maxwell et al., 2014). One of the most applied models to describe the K under unsaturated conditions and the soil water saturation (S) as a function of the matric potential is the van Genuchten model (van Genuchten, 1980). Although some of the parameters of this model have a certain physical meaning, such as $\alpha\ [L^{-1}]$, which is approximately the inverse of the air-entry value, and $n\ [-]$, which is related to the pore size distribution (Vereecken et al., 2010), it is still an empirical model, hindering the direct determination of these parameters. Therefore, they are usually derived from inverse modeling based on, for example, soil moisture observations. This presents a challenge for IHMs, as automated calibration is uncommon for such models due to high computational costs (Engdahl, 2024). Consequently, the determination of α and n in the context of IHMs usually relies on literature values or on the use of surrogate models (Bogena et al., 2013; Koch et al., 2016).

An additional aspect, often overlooked in IHMs coupled to land surface models, are parameters that characterize the interaction between soil and vegetation under unsaturated conditions, such as field capacity (S_{fc}) and the wilting point (S_{wp}). In agricultural sciences, these parameters are typically defined as volumetric water content at a specific matric potential, where the field capacity corresponds to the water content at a suction of 3.3 m and the wilting point at 150 m (Assi et al., 2019), although these definitions actually depend on soil texture and plant physiology (Ibrahimi & Alghamdi, 2022). Both parameters are strongly linked to the soil water retention curve (SWRC) defined by the van Genuchten parameters. This fact is frequently neglected in IHMs, which may have significant implications for the determination of soil moisture, an important variable that can also be used as reference figure during model calibration (Vereecken et al., 2014). As presented in Srivastava et al. (2014) and Jefferson et al. (2015) for IHM applications, S_{fc}, S_{wp} and van Genuchten parameters are expected to have a significant influence on streamflow generation and evapotranspiration, especially under water limited conditions, because they determine the vegetation water stress function, which uses the aggregated moisture availability over the root zone and controls transpiration fluxes (Ferguson et al., 2016).

To identify interactions and the most influential parameters among the above mentioned and others, modelers need to perform sensitivity analyses. Global sensitivity analyses (GSAs) are particularly useful before calibration because they capture nonlinearities and parameter interactions across the entire parameter space. However, formal GSAs require hundreds to thousands of model evaluations, which makes them very challenging for IHMs. A few studies (e.g., Srivastava et al. (2014); Jaros et al. (2019); Maples et al. (2020)) have nevertheless applied GSAs for real hydrological settings and provided valuable insights. Based on 340 simulations of an assumed isotropic subsurface, Srivastava et al. (2014) showed that sensitivities vary spatially within a basin: elevated regions were controlled by the K of confining units while lower lying regions by the K of regional aquifers. Furthermore, peak flows were sensitive to Manning's coefficients of the streams in the upper catchment area, and unsaturated flow parameters became more influential under water-limited conditions. In another study, Jaros et al. (2019) identified K and anisotropy ratios as the predominant controlling parameters on the basis of 1,180 steady-state simulations of a boreal Esker-Aapa mire system, while also highlighting variable contributions from other parameters, including those defining SWRCs. Together, these studies demonstrate the value of GSAs for

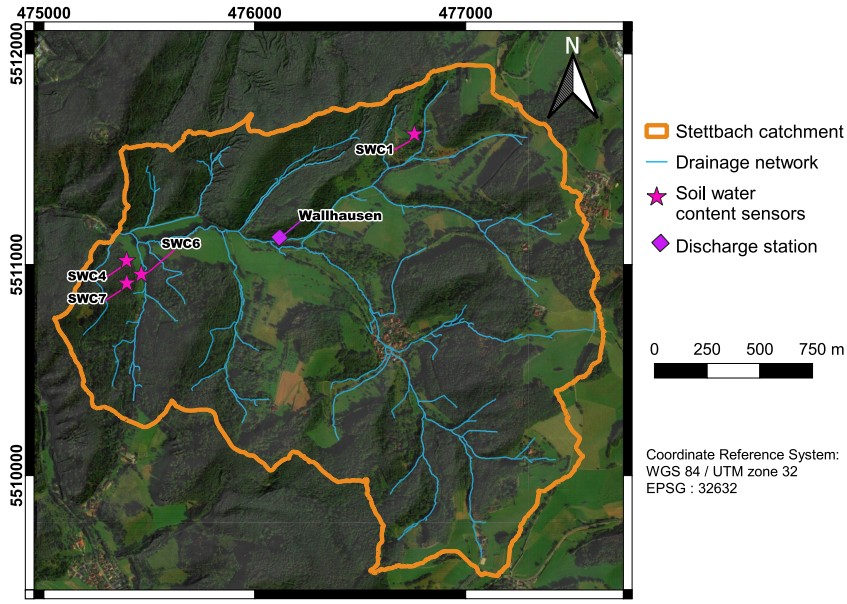

Figure 1. Study area and instrumentation.

identifying key parameters and their interactions in real systems, but also emphasize their high computational demand and thus the need of using simplified schemes.

Therefore, we adopted an approach based on a parametric sensitivity analysis designed to capture the key aspects of saturated and unsaturated flow parameters while relying on a reduced number of simulations. Thus, this study aims to deepen our understanding of the influence of K under both saturated and unsaturated conditions within the context of an IHM. To achieve this, we used a variably saturated numerical hydrological model coupled with a land surface model (Parflow-CLM) to simulate the water cycle in the critical zone of a 4.0 km^2 large headwater catchment in the Odenwald, Germany. We first defined 15 different isotropic K parametrizations for two different porosities of the shallow geological horizons, with a simplified subsurface conceptualization. These were evaluated according to observations of stream discharge to analyze the model performance at different temporal resolutions. Subsequently, anisotropy was introduced in the near-surface geological horizons for selected scenarios to understand its effect on streamflow generation and groundwater level distribution. For a plausible scenario according to streamflow, we analyzed the model sensitivity regarding soil moisture distribution with respect to the SWRC and considering different definitions of field capacity and wilting point. Finally, our simulations were compared to observations of soil moisture in the first meter of specific locations in forests and grasslands over time to investigate the effect of the selected parameters (S_{fc}, S_{wp}, α, n) over different seasons. Based on our results, we provide insights into parameter sensitivities with respect to different output variables and offer recommendations for parameter optimization and parameter ranges, especially for Unconsolidated Deposits (U.D.), within the framework of IHMs.

2. Methods

2.1. Study Area

The model domain comprises the headwater catchment of the Stettbach river (Figure 1), which is located in the low mountain range of the Odenwald in Germany. It has an area of 4.0 km^2 and the elevation ranges between 195 and 440 m a.s.l. The site was selected because of its low human intervention on the hydrological system, with forests and grasslands being the main land uses of the area. In the catchment we installed a discharge station in one of the tributaries of the Stettbach river, the Bach von Wallhausen, hereinafter referred to as Wallhausen stream, and four SoilNet wireless sensor systems (Bogena et al., 2010, 2022) to measure the volumetric soil water content (SWC) at six depths of the first meter of soil (at 5; 10; 20; 40; 60, and 80 cm b.g.l.) for each system (Figure 1).

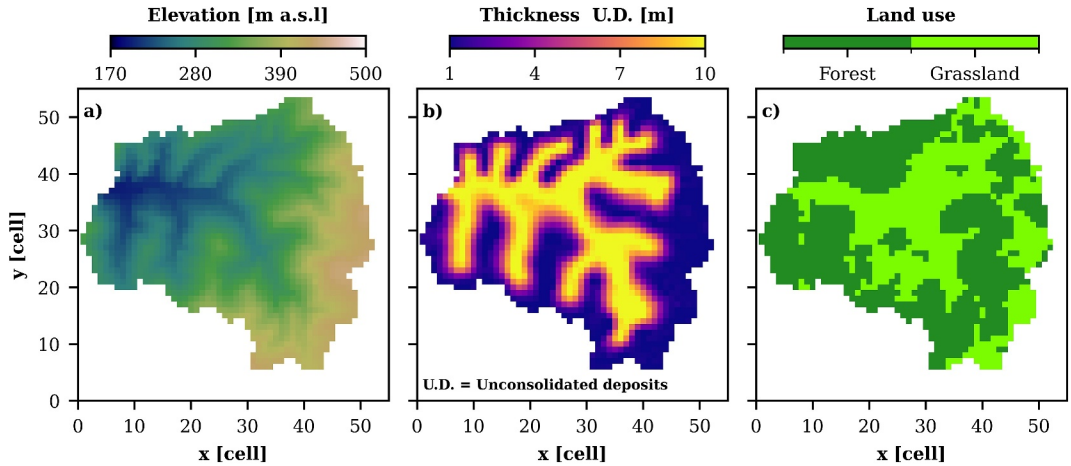

Figure 2. Data used for model geometry (a, b) and land use parameter distribution (c) for the Parflow-CLM models.

According to the Köppen-Geiger classification, the climate in this region is categorized as temperate oceanic (Peel et al., 2007), generally characterized by mild winters and summers. The warmest months are June, July and August and the coldest months are January, February and December. For the years 2021, 2022, and 2023, which are the focus of this work, the annual mean temperatures were 9.9, 11.6, and 11.7°C, respectively. Annual sums of precipitation were 872, 785, and 1,092 mm for the same years. Monthly weather variables for these years are presented in Figure S1 in Supporting Information S1. Geologically, the catchment belongs to the northeastern part of the Flasergranitoid zone in the Odenwald Crystalline Complex (Dörr & Stein, 2019), which consists mainly of plutonic rocks (granites) and to a lesser degree of metamorphic rocks (amphibolites), both with high degrees of weathering in its upper parts (Stein, 2001). These rock units are overlaid by unconsolidated deposits in which brown earths, colluvial soils and gley soils, consisting mainly of silty and sandy loam soils have been developed. In slope depressions, that is, morphologically lower-lying zones, there are mainly gravelly-sandy sediments of alluvial deposits, with the total thickness of the unconsolidated deposits ranging from a few decimeters to 10–20 m (HLNUG, 2017).

2.2. Numerical Tools and Model Geometry

The IHM used in this study is the Parflow-Common Land Model (PF-CLM) version 3.12.0. Briefly, PF solves the Richard's equation in a three-dimensional subsurface domain, incorporating a two-dimensional kinematic wave equation as approximation of overland water flow (Kollet & Maxwell, 2006). The coupling with land surface processes is realized with a modified version of the original CLM that is called as a subroutine within PF to compute energy and water fluxes, such as evaporation and transpiration (Kuffour et al., 2020). A detailed description of the equations that define PF-CLM can be found in Jefferson et al. (2015).

A digital elevation model with a resolution of 1 m was obtained from the Hessian Agency for Land Management and Geoinformation (HVBG, 2024b) and resampled to a 50 m grid, same as for the land use (HVBG (2024a); Figures 2a and 2c). The meteorological information required as input for the model was obtained from nearby stations of the German Weather Service (DWD, 2024), located in the city of Michelstadt, 25 km from the study area.

Due to the absence of boreholes in the study area, we had to develop a simplified geological model based on own field investigations and analogies to comparable areas. Based on shallow manual drilling and two geoelectrical profiles, we have estimated a thickness of alluvial and colluvial deposits of 1 m in the upslope areas and 10 m in the depressions, which was regionalized based on topographic features such as slope, curvature and upslope contribution in analogy to Schulz et al. (2013) (Figure 2b). The sediments were grouped to one hydrogeological unit, which we termed Unconsolidated Deposits (U.D.). Moreover, we assumed a unit of weathered rock (W.R.) with a thickness of 5 m underlying the U.D., representing both saprolite and fissured rock layers commonly found in hard rock formations (Lachassagne et al., 2021). This simplification arises from the lack of site-specific data on the weathering zone, which in the Odenwald generally ranges from 5 to 10 m but can locally reach up to 20 m

Table 1
Hydrogeological Units and Vertical Discretization of PF-CLM Models

Hydrogeological unit	Unconsolidated deposits (U.D.)	Weathered rock (W.R.)	Bedrock (bed)
Description	Soil, colluvial and alluvial deposits	Saprolite and fissured rock layer	Low permeability rock
Thickness [m]	From 1 to 10	5	From 110 to 119
Vertical grid size [m]	From 0.03 to 0.5	0.5	From 0.5 to 60

(HLNUG, 2017). Below the W.R., we defined a unit of Bedrock with a variable thickness that the total thickness of the model is 125 m. A summary of the assumed hydrogeological units is presented in Table 1. Finally, we used this geological conceptual subsurface model domain to build the vertical numerical grid of the PF-CLM models.

The numerical domain of the PF-CLM models have a dimension of 2,750 × 3,000 m, with a constant horizontal grid resolution of 50 m, resulting in 60 rows and 55 columns. We selected this resolution as a trade-off between preserving slope representation and limiting the number of cells. Areas that do not drain into the Stettbach catchment were excluded from the active domain. The subsurface domain was discretized in 40 layers with an increasing thickness from the surface of the model to the bottom, starting with 0.03 m at the top of the U.D. unit until 60 m for the lowest Bedrock layer (Table 1). To decrease the number of active cells in the vertical direction, a terrain following grid was used (Maxwell, 2013). The three-dimensional geometry (Figure 3), numerical grid and an initial PF-CLM run file were established using the open-source software PFGIS-Tool v1.0.0 (Carlotto et al., 2023). We assumed a no-flow boundary condition at the lateral catchment boundaries and the bottom of the domain. For the top of the model, we set an overland flow condition. Furthermore, we defined the coupling of PF and CLM over the first seven layers of the domain, equivalent to 1 m, allowing for temperature exchange and root water uptake.

For spin-up, we first determined the spin-up time by running preliminary models with the meteorological forcing of the year 2020 in a loop. Eight to 10 years were required to stabilize the surface and subsurface storage, which is in accordance with former studies analyzing spin-up of PF-CLM models (Seck et al., 2015). To avoid being biased by the specific hydrologic conditions of the year 2020, we subsequently initialized all models with a water table at 2 m b.g.l. and ran them for 15 years with the meteorological forcing of the years 2006–2020 as spin-up period. We then focused on the simulated results for the years 2021–2023 for model evaluation.

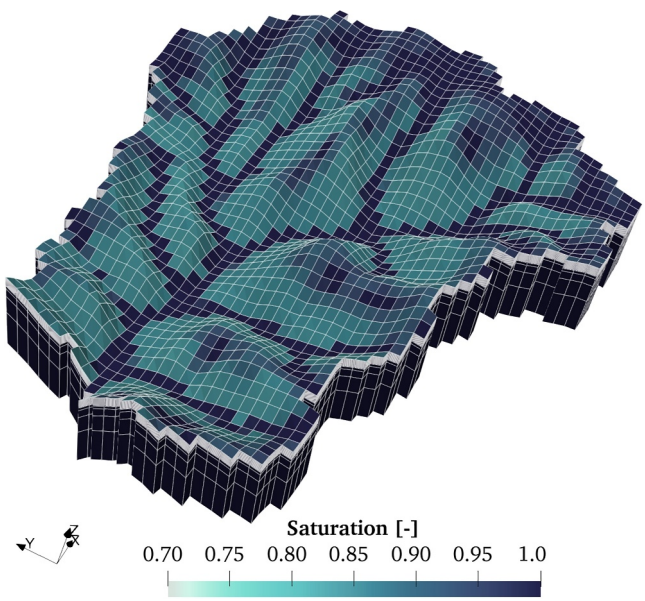

Figure 3. Three-dimensional terrain following grid used for Parflow-CLM models depicting simulated drainage network during a day in winter (7 January 2022). Vertical scale is amplified by a factor of 3 for better visualization.

2.3. Modeling Approach

A very crucial part of setting up IHMs is the parametrization of the *K*-values. The fact that *K*-fields are commonly scaled in IHMs because of grid resolution and the associated loss of topographic information (Fang et al., 2016; Foster, 2018; Schalge et al., 2019; Soltani et al., 2022), does not allow the direct use of typical a priori estimates from hydraulic tests or literature. Moreover, *K*-fields are also impacted by aspects such as anisotropy and unsaturated parametrization. To assess the impact of *K* in conjunction with the other influencing factors mentioned above, we developed a modeling approach using a limited number of simulations, necessitated by the high computational costs of this type of model. We present an overview of our approach in Figure 4, with further details provided later in this section. A summary of all performed numerical experiments with a total of 55 simulations is presented in Table 2. All models were run on a workstation with a 64-cores AMD EPYC 7713 processor (2.0 GHz base clock) and 256 GB DDR4 RAM. Depending on the parameter configuration, running times using all cores varied between 3 and 10 days for the 18 years simulation period, which included 15 years of spin-up plus 3 years of simulation for each experiment.

We started with 15 isotropic exploratory simulations spanning several orders of magnitude for the *K*-values (Stage I in Figure 4 and Table 2), mainly for the U. D and W.R. units, including scenarios where we assumed a homogeneous

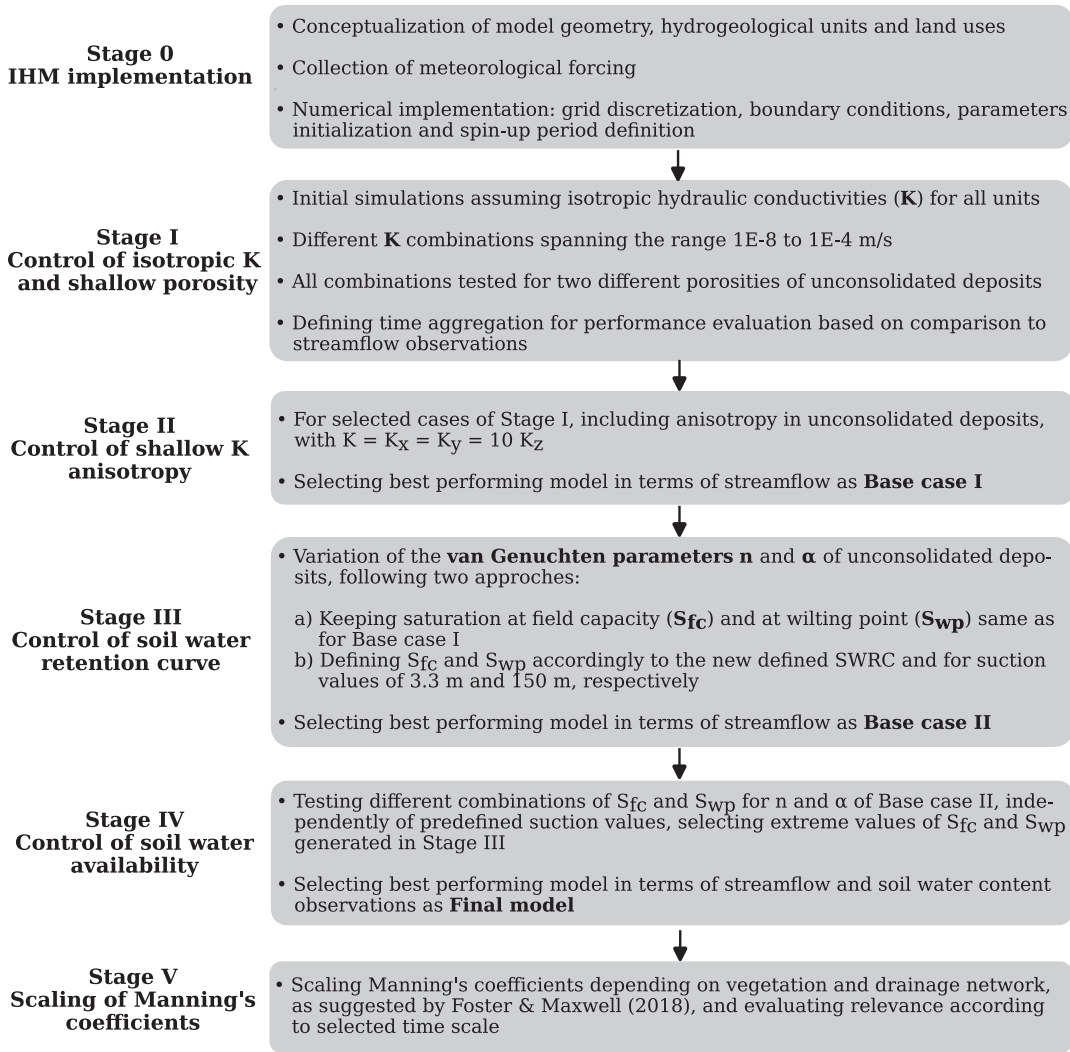

Figure 4. Modeling approach.

K-value of the whole domain (Figure S2 in Supporting Information S1). Besides these homogeneous cases, the K-value of the Bedrock was set to 10^{-8} m/s, beyond which groundwater flow is assumed negligible (Rapp et al., 2020). In addition to analyzing the impact of K, we used this first series of simulations to explore a reasonable temporal resolution for the performance evaluation, that is, comparing simulated with observed variables. To avoid the need for additional model runs for this purpose, we carried out all simulations with one-hour time steps and subsequently performed a temporal aggregation by calculating moving averages of the time series using different kernel sizes with daily, weekly and monthly windows.

As one of our objectives is to understand the influence of unsaturated parameters, we tested two different values for the porosity, that is, saturated water content (ϕ), of the U.D. for the 15 isotropic models. We defined a $\phi^{U.D}$ of 0.50 and 0.42, which relates to sediments with fine and medium particle sizes, respectively (Stage I in Figure 4 and Table 2). For both cases we kept the same van Genuchten parameters, that is $n = 1.4$ and $\alpha = 1.5$ [1/m], which were calculated as geometric and arithmetic mean, respectively, for sandy loam and silt loam defined by the USDA soil texture using Rosseta3 (Zhang & Schaap, 2017). The porosities of the W.R. and Bedrock were kept constant for all experiments, with $\phi^{W.R} = 0.25$ and $\phi^{Bed} = 0.05$, respectively.

Based on the comparison of the results from these 30 simulations with the observed discharges for the period between 2021 and 2023, we selected four scenarios per porosity (Stage II in Figure 4 and Table 2). For these eight simulations, we applied an anisotropy factor (the ratio between horizontal and vertical K) of 10, which is a

Table 2
Summary of Numerical Experiments and Related Hydraulic Parameter Values

Experiment	$K^{U.D.}$ [m/s]	$K^{W.R.}$ [m/s]	K^{Bed} [m/s]	$k_z^{U.D.}$ [-]	$\phi^{U.D.}$ [-]	$\alpha^{U.D.}$ [1/m]	$n^{U.D.}$ [-]	S_{fc} [-]	S_{wp} [-]	Description
E01	1E−7	1E−7	1E−7	1.0	0.50	1.5	1.40	0.53	0.15	Stage I Isotropic cases of homogeneous K in the entire domain
E02	1E−6	1E−6	1E−6	1.0	0.50	1.5	1.40	0.53	0.15	
E03	1E−5	1E−5	1E−5	1.0	0.50	1.5	1.40	0.53	0.15	
E04	1E−7	1E−8	1E−8	1.0	0.50	1.5	1.40	0.53	0.15	Stage I Isotropic cases with $K^{W.R.} = K^{Bed} = 1E{-}8$ m/s
E05	1E−6	1E−8	1E−8	1.0	0.50	1.5	1.40	0.53	0.15	
E06	1E−5	1E−8	1E−8	1.0	0.50	1.5	1.40	0.53	0.15	
E07	1E−7	1E−8	1E−8	1.0	0.50	1.5	1.40	0.53	0.15	Stage I Isotropic cases with $K^{W.R.} = 0.1K^{U.D.}$
E08	1E−6	1E−7	1E−8	1.0	0.50	1.5	1.40	0.53	0.15	
E09	1E−5	1E−6	1E−8	1.0	0.50	1.5	1.40	0.53	0.15	
E10	1E−7	1E−7	1E−8	1.0	0.50	1.5	1.40	0.53	0.15	Stage I Isotropic cases with $K^{W.R.} = K^{U.D.}$
E11	1E−6	1E−6	1E−8	1.0	0.50	1.5	1.40	0.53	0.15	
E12	1E−5	1E−5	1E−8	1.0	0.50	1.5	1.40	0.53	0.15	
E13	1E−7	1E−6	1E−8	1.0	0.50	1.5	1.40	0.53	0.15	Stage I Isotropic cases with $K^{W.R.} = 10K^{U.D.}$
E14	1E−6	1E−5	1E−8	1.0	0.50	1.5	1.40	0.53	0.15	
E15	1E−5	1E−4	1E−8	1.0	0.50	1.5	1.40	0.53	0.15	
E16	1E−7	1E−7	1E−7	1.0	0.42	1.5	1.40	0.53	0.15	Stage I Same isotropic experiments as E01 to E15 but with $\phi^{U.D.} = 0.42$ instead of $\phi^{U.D.} = 0.50$
E17	1E−6	1E−6	1E−6	1.0	0.42	1.5	1.40	0.53	0.15	
E18	1E−5	1E−5	1E−5	1.0	0.42	1.5	1.40	0.53	0.15	
E19	1E−7	1E−8	1E−8	1.0	0.42	1.5	1.40	0.53	0.15	
E20	1E−6	1E−8	1E−8	1.0	0.42	1.5	1.40	0.53	0.15	
E21	1E−5	1E−8	1E−8	1.0	0.42	1.5	1.40	0.53	0.15	
E22	1E−7	1E−8	1E−8	1.0	0.42	1.5	1.40	0.53	0.15	
E23	1E−6	1E−7	1E−8	1.0	0.42	1.5	1.40	0.53	0.15	
E24	1E−5	1E−6	1E−8	1.0	0.42	1.5	1.40	0.53	0.15	
E25	1E−7	1E−7	1E−8	1.0	0.42	1.5	1.40	0.53	0.15	
E26	1E−6	1E−6	1E−8	1.0	0.42	1.5	1.40	0.53	0.15	
E27	1E−5	1E−5	1E−8	1.0	0.42	1.5	1.40	0.53	0.15	
E28	1E−7	1E−6	1E−8	1.0	0.42	1.5	1.40	0.53	0.15	
E29	1E−6	1E−5	1E−8	1.0	0.42	1.5	1.40	0.53	0.15	
E30	1E−5	1E−4	1E−8	1.0	0.42	1.5	1.40	0.53	0.15	
E31	1E−6	1E−6	1E−8	0.1	0.50	1.5	1.40	0.53	0.15	Stage II Anisotropic variations for selected isotropic cases. Anisotropic experiments consider a decrease of K only in the vertical direction, that is, $K_z^{U.D.} = k_z^{U.D.}K^{U.D.}$ and $K_x^{U.D.} = K_y^{U.D.} = K^{U.D.}$
E32	1E−6	1E−5	1E−8	0.1	0.50	1.5	1.40	0.53	0.15	
E33	1E−5	1E−8	1E−8	0.1	0.50	1.5	1.40	0.53	0.15	
E34	1E−5	1E−6	1E−8	0.1	0.50	1.5	1.40	0.53	0.15	
E35	1E−6	1E−6	1E−8	0.1	0.42	1.5	1.40	0.53	0.15	
E36	1E−6	1E−5	1E−8	0.1	0.42	1.5	1.40	0.53	0.15	
E37	1E−5	1E−8	1E−8	0.1	0.42	1.5	1.40	0.53	0.15	
E38	1E−5	1E−6	1E−8	0.1	0.42	1.5	1.40	0.53	0.15	
E39	1E−5	1E−6	1E−8	0.1	0.42	0.9	1.40	0.53	0.15	Stage III Experiments varying $\alpha^{U.D.}$ and $n^{U.D.}$ keeping defined S_{fc} and S_{wp} as in previous experiments
E40	1E−5	1E−6	1E−8	0.1	0.42	2.6	1.40	0.53	0.15	
E41	1E−5	1E−6	1E−8	0.1	0.42	1.5	1.35	0.53	0.15	
E42	1E−5	1E−6	1E−8	0.1	0.42	1.5	1.60	0.53	0.15	
E43	1E−5	1E−6	1E−8	0.1	0.42	2.6	1.60	0.53	0.15	
E44	1E−5	1E−6	1E−8	0.1	0.42	0.9	1.35	0.53	0.15	

Table 2
Continued

Experiment	$K^{U.D.}$ [m/s]	$K^{W.R.}$ [m/s]	K^{Bed} [m/s]	$k_z^{U.D.}$ [-]	$\phi^{U.D.}$ [-]	$\alpha^{U.D.}$ [1/m]	$n^{U.D.}$ [-]	S_{fc} [-]	S_{wp} [-]	Description
E45	1E−5	1E−6	1E−8	0.1	0.42	0.9	1.40	0.63	0.18	
E46	1E−5	1E−6	1E−8	0.1	0.42	2.6	1.40	0.44	0.13	
E47	1E−5	1E−6	1E−8	0.1	0.42	1.5	1.35	0.57	0.18	Stage III Experiments varying $\alpha^{U.D.}$ and $n^{U.D.}$ updating S_{fc} and S_{wp} as saturations at defined suction values
E48	1E−5	1E−6	1E−8	0.1	0.42	1.5	1.60	0.40	0.08	
E49	1E−5	1E−6	1E−8	0.1	0.42	2.6	1.60	0.30	0.07	
E50	1E−5	1E−6	1E−8	0.1	0.42	0.9	1.35	0.66	0.21	
E51	1E−5	1E−6	1E−8	0.1	0.42	0.9	1.35	1.00	0.10	
E52	1E−5	1E−6	1E−8	0.1	0.42	0.9	1.35	0.30	0.21	Stage IV Experiments with different combinations of S_{fc} and S_{wp} for a defined set of $\alpha^{U.D.}$ and $n^{U.D.}$
E53	1E−5	1E−6	1E−8	0.1	0.42	0.9	1.35	0.66	0.07	
E54	1E−5	1E−6	1E−8	0.1	0.42	0.9	1.35	0.30	0.07	
E55	1E−5	1E−6	1E−8	0.1	0.42	0.9	1.35	0.30	0.07	Stage V Experiment E54 with scaled Manning's coefficients according to Foster, 2018

Note. Note that experiments E07 and E22 correspond to E04 and E19, respectively. Experiments in bold constitute benchmark cases.

commonly used a priori estimate for layered aquifers (Bakker & Bot, 2024). The anisotropic model, performing best in terms of Nash-Sutcliffe efficiency (NSE) and Kling-Gupta efficiency (KGE) for observed discharges, is defined as "Base case I" (experiment E38 in Table 2) and constitutes the starting point for variations in unsaturated flow parameters.

For changing unsaturated parameters of the U.D. unit, we followed two approaches (Stage III in Figure 4 and Table 2). First, we ran six simulations, in which we varied n and α (hereinafter referred to as van Genuchten parameters), keeping the same S_{fc} and S_{wp} as defined for the Base case I scenario, that is, with soil saturations at suctions of 3.3 and 150 m, respectively. For $n = 1.4$ and $\alpha = 1.5$ [1/m], this resulted in $S_{fc} = 0.53$ and $S_{wp} = 0.15$. Second, using the same van Genuchten parameters as in the first approach, we also changed S_{fc} and S_{wp} according to the soil water retention curves established with each new combination of n and α. With this, we aimed to understand the effects of the van Genuchten parameters n and α, as well as S_{fc} and S_{wp} separately. Afterward, we selected the best performing scenario in terms of discharge, yielding "Base case II" (experiment E44 in Table 2). To additionally test the impact of the definitions of S_{fc} and S_{wp}, we performed four further simulations (Stage IV in Figure 4 and Table 2) in which we only varied S_{fc} and S_{wp} for a defined set of n and α ($n = 1.35$ and $\alpha = 0.9$ [1/m]), relaxing their previous definitions, that is, S_{fc} and S_{wp} as soil saturations at a matric potential of 3.3 and 150 m, respectively. Afterward, we compared the simulated soil water contents to our observations. We selected the model that best reproduced the observations of the weighted average of saturations in the first meter of soil as our "Final model" (Experiment 54 in Table 2). Finally, as an additional exploration for improving the model performance regarding streamflow, we performed a scaling of the Manning's coefficients of the "Final model" according to Foster, 2018 (Stage V in Figure 4 and Table 2).

3. Results and Discussion

3.1. Performance of Isotropic Conceptual Models

The performance of the 15 isotropic models at different time scales, in terms of NSE and KGE, are shown in Figure 5 for the case $\phi^{U.D.} = 0.42$ and in Figure S3 in Supporting Information S1 for $\phi^{U.D.} = 0.50$, without considerable differences among both porosities. It is evident that the choice of the time scale has an important effect on the performance evaluation of simulations and consequently on the selection of plausible scenarios. The evaluation at an hourly time scale does not show simulations with satisfying results. This difficulty of modeling streamflow for IHMs at an hourly time scale has already been pointed out in previous studies (Foster, 2018). At both monthly and weekly scales, several models still show acceptable performance, making it difficult to

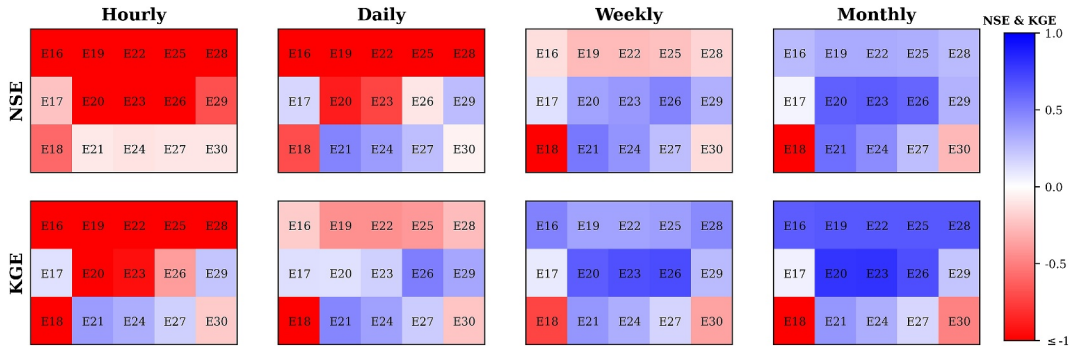

Figure 5. Performance evaluation at different time scales of isotropic models with $\phi^{U.D.} = 0.42$ for discharges of the Wallhausen stream during the years 2021–2023. For description of the numerical experiments the reader is referred to Table 2.

constrain the space of possible solutions. Therefore, we selected a daily scale to evaluate our simulations. Additionally, there are important differences between the selected criteria (e.g., E26 at daily scale, Figure 5), which can be explained by the fact that the NSE only considers deviations from a mean, whereas the KGE also includes correlation information (Gupta et al., 2009). This emphasizes the value of evaluating hydrological models using more than one performance criterion. Figures S4 and S5 in Supporting Information S1 present the specific components of the KGE at daily resolution. The results indicate that the relative variability error (a) generally exhibits the poorest performance.

To better discriminate between the simulations with the 15 different isotropic K parametrizations of the three hydrogeological units as well as the two assumptions for porosity of the U.D., the distribution of observed and simulated flows at daily resolution, sorted by median discharge, is presented in Figure 6. Interestingly, almost all models exhibited similar mean flow rates close to the observed one, with the exception of scenarios with a very high K in the whole domain (E03/E18, E02/E17) or in the U.D. and W.R. units (E15/E30), which can be explained by quick vertical drainage into deeper layers under these conditions and the resulting lower water table, causing groundwater drainage downstream of the discharge station (Figures S6 to S9 in Supporting Information S1). Models with relatively low K in the U.D. and W.R. (E04/E19, E10/E25, E13/E28, E01/E16, E05/E20, and E08/E23) present a broader distribution of streamflow due to more extensive saturated areas in winter resulting in saturation excess overland flow (Figures S7 and S9 in Supporting Information S1), which in turn implies less subsurface storage and consequently lower discharges in warm and dry periods, that is, lower or inexistent base flow in summer (time series of simulated discharge are presented in Figures S4 and S5 in Supporting Information S1). Conversely, scenarios with high K-values in the two upper hydrogeological units (E02/E17, E11/E26, E15/E30, E14/E29, E06/E21, E09/E24, and E12/E27) show lower maximum streamflow, but consistently base flow, a characteristic that is also present in the observed discharge. These findings are consistent with previous studies (Foster, 2018; Rapp et al., 2020), which have also shown that a relatively high K, particularly in shallow horizons, increases base flows while decreasing peak flows.

The isotropic models show an influence of the K of the W.R. on discharges for all studied parametrizations of the U.D. This is inferred by comparing models with same $K^{U.D.}$ and $K^{Bedrock} = 10^{-8}$ m/s, but with different $K^{W.R.}$, such as models E04/E19, E10/E25 and E13/E28 with $K^{U.D.} = 10^{-7}$ m/s, models E05/E20, E08/E23, E11/E26, E14/E29 with $K^{U.D.} = 10^{-6}$ m/s, as well as models E06/E21, E09/E24, E12/E27 and E15/E30 with $K^{U.D.} = 10^{-5}$ m/s (Figure 6 and S2 in Supporting Information S1 and Table 2). In most cases, higher $K^{W.R.}$ values result in a narrower distribution of streamflow, with a more consistent presence of base flow (Figure 6; Figures S4 and S5 in Supporting Information S1), which is also shown by the more extensive drainage network during summer (Figures S6 and S8 in Supporting Information S1). This can be explained by a higher subsurface lateral transfer in the W.R. in winter, which feeds the downstream saturated areas and promotes faster drainage, resulting in less saturation-excess overland flow (Figures S7 and S9 in Supporting Information S1).

Simulated streamflow in the Wallhausen stream did not present considerable variations at different $\phi^{U.D.}$ (Figure 6). There is a tendency for lower $\phi^{U.D.}$ to result in slightly higher discharge maximums and slightly lower

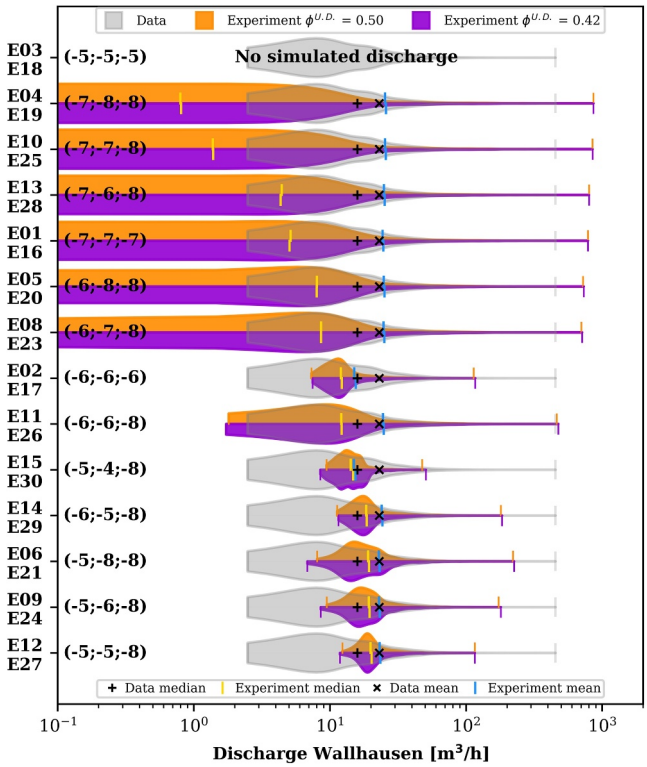

Figure 6. Probability density functions of observed and simulated streamflow distributions at daily resolution for the 15 isotropic conceptual models with both U.D. porosities. Values in parenthesis show the log K [m/s] of the units U.D., weathered rock and Bedrock for each experiment, respectively. Discharges are in logarithmic scale for better visualization of its distribution. For description of the numerical experiments the reader is referred to Table 2.

minimums, especially for cases with high $K^{U.D.}$, indicating that a lower storage in the U.D. unit leads to higher runoff during strong precipitation events, and to a lower base flow during the dry season, albeit both to a small extent. The low sensitivity of streamflow to the porosity of shallow layers was also observed by Fang et al. (2015) in a smaller catchment of 0.4 km^2. It is expected that the effects of porosity could be more relevant for bigger basins, where relative differences in porosity correspond to larger total amounts of water that could be stored in shallow soil horizons.

Based on the performance criteria KGE and NSE and the ability to depict the base flow, we selected the models E11/E26, E14/E29, E06/E21, and E09/E24 to explore the role of anisotropy.

3.2. Influence of Shallow Anisotropy

The effects of including vertical anisotropy in the U.D. unit for the selected scenarios with $\phi^{U.D.} = 0.42$ and $\phi^{U.D.} = 0.50$ are shown in Figure 7 and Figures S10 in Supporting Information S1, respectively. A substantial change is observed for the models with $K_x^{U.D.} = K_y^{U.D.} = 10^{-6}$ m/s (E11/E26 and E14/E29) and to a lesser degree for the models with $K_x^{U.D.} = K_y^{U.D.} = 10^{-5}$ m/s (E06/E21 and E09/E24). For E26 and E29, which just differ in the K of the W.R. unit, the incorporation of anisotropy, with $K_z^{U.D.} = 10^{-7}$ m/s, makes both cases resulting in a very similar distribution of simulated streamflow (Figure 7). These distributions are almost identical to the isotropic cases with $K^{U.D.} = 10^{-7}$ m/s (E16, E20, E25, and E28; Figure 6). Interestingly, for E21 and E24, which also just differ in the K of the W.R. unit, incorporating vertical anisotropy, that is, $K_z^{U.D.} = 10^{-6}$ m/s, again leads for both scenarios to the same discharge distribution. However, in this case not to the same behavior as in the isotropic cases with the same vertical $K^{U.D.}$ of 10^{-6} m/s (E17, E20, E23, E24 and E29). Taken together, these observations suggest that in cases with a low K-value, the vertical component of $K^{U.D.}$ controls the discharge, which, however, is no longer the case at higher K-values. Similar conclusions were reached by Herzog et al. (2021) using a different conceptual model for a hard rock aquifer in West Africa, which did not account for anisotropy in the shallow horizons. These findings underscore the importance of performing sensitivity analyses for K in shallow geological formations. Moreover, understanding the effects of considering anisotropy of K, especially of the upper soil layers for simulations with IHMs, seems to be important. This is confirmed by findings of Jaros et al. (2019), where in a GSA of a steady state IHM of an Esker-Aapa mire system in Finland, anisotropy ratios of sandy soils were among the most sensitive parameters.

To further explore the effect of anisotropy in U.D., we analyzed the simulated groundwater table depths for the day of highest (07/January/2022) and lowest (05/August/2022) observed discharge, hereinafter referred to as "winter" and "summer," respectively (Figures 8 and 9). For both seasons, the spatial distribution of the groundwater table is practically the same for anisotropic cases with equal $K_z^{U.D}$. For the corresponding isotropic cases, however, they are always different, which is in line with the conclusions derived from the statistical streamflow distributions. For all cases and in both seasons, the incorporation of anisotropy, that is, decreasing the vertical K of the U.D. unit, resulted in a shallower groundwater table, same as concluded in Rapp et al. (2020). This strong influence of anisotropy on the various model results suggests that the parametrization of anisotropy should be calibrated rather than taken as a fixed value (Bakker & Bot, 2024; Shepley, 2024), which poses a challenge for IHMs due to the large computing times. The sensitivity of the groundwater levels with respect to anisotropy also suggests using them as a reference figure during calibration, as demonstrated in Engdahl (2024).

Similar to the isotropic scenarios, the main difference between the two assumed porosities is that for $\phi^{U.D.} = 0.42$, the simulated discharge exhibits a lower minimum and a higher maximum than in cases with $\phi^{U.D.} = 0.50$ (Figure 7 and Figures S10 in Supporting Information S1), which is due to less water storage in that unit. Until this point, the scenarios that statistically perform best in simulating the discharge are the anisotropic

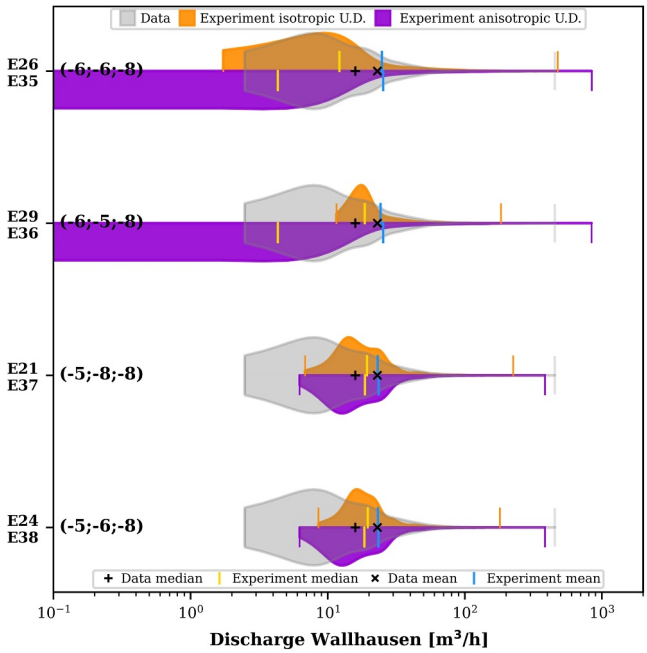

Figure 7. Probability density functions of observed and simulated streamflow distributions at daily resolution for selected isotropic and anisotropic experiments with $\phi^{U.D.} = 0.42$. Values in parenthesis show the log K_x [m/s] of the units U.D., weathered rock (W.R.) and Bedrock for each case. For anisotropic cases, the units W.R. and Bedrock are isotropic ($K_x = K_y = K_z$) and in U.D. $K_x = K_y = 10K_z$. For description of the numerical experiments the reader is referred to Table 2.

scenarios with $\phi^{U.D.} = 0.42$ (E37 and E38), both with a NSE of 0.54 and KGE of 0.65, due to their exact same behavior despite a different $K^{W.R.}$ value. Based on this, we arbitrarily selected the experiment E38, hereinafter referred to as "Base case I" (Figure 4), as starting point to investigate the influence of unsaturated parameters in our model.

3.3. Influence of Unsaturated Flow Parameters

Simulated volumetric soil water contents integrated over the uppermost 1 m for the Base case I model exhibit strong seasonal variations throughout the catchment (Figure 10). During winter, upslope areas with low topographic gradients, which are conceptualized with a thin U.D. unit (see Figures 2a and 2b), show conditions close to total saturation. In contrast, lower slopes with a thicker U.D. have a comparatively lower but still high water content, except in the cells where the subsurface system is drained. During summer, the behavior is completely different. Generally, the upper part of soil is much drier and the distribution of the SWC follows the pattern of land use, with significantly lower values in forest areas compared to grasslands (Figure 2c). Accordingly, a smaller drainage network develops in the catchment during summer. The presence of this drainage network even in summer also shows the existence of permanent base flow in the streamflow simulation, which is consistent with the observations.

For the analysis of unsaturated parameters, we focused on the upper model layers, that is, the U.D. unit. For this purpose, we derived a variation for the van Genuchten parameters α and n, based on the mean and standard deviation estimates of Rosseta3 (Zhang & Schaap, 2017) for a sandy loam texture, yielding $n_{min} = 1.35$, $n_{max} = 1.60$, $\alpha_{min} = 0.9$ [1/m] and $\alpha_{max} = 2.6$ [1/m]. At the same time, we conducted a literature review of van Genuchten parameter values used in the context of PF-CLM applications for near-surface geological units (see Figure S11 and Table S1 in Supporting Information S1). This shows that our selected range encompasses a spectrum of comparatively low values, corresponding to a finer soil texture. Figure 11 presents selected SWRC, derived from the range of α and n. This controlled variation of van Genuchten parameters intended to keep physically realistic SWRCs, an aspect also highlighted by Jaros et al. (2019), when sampling randomly α and n in a defined parameter

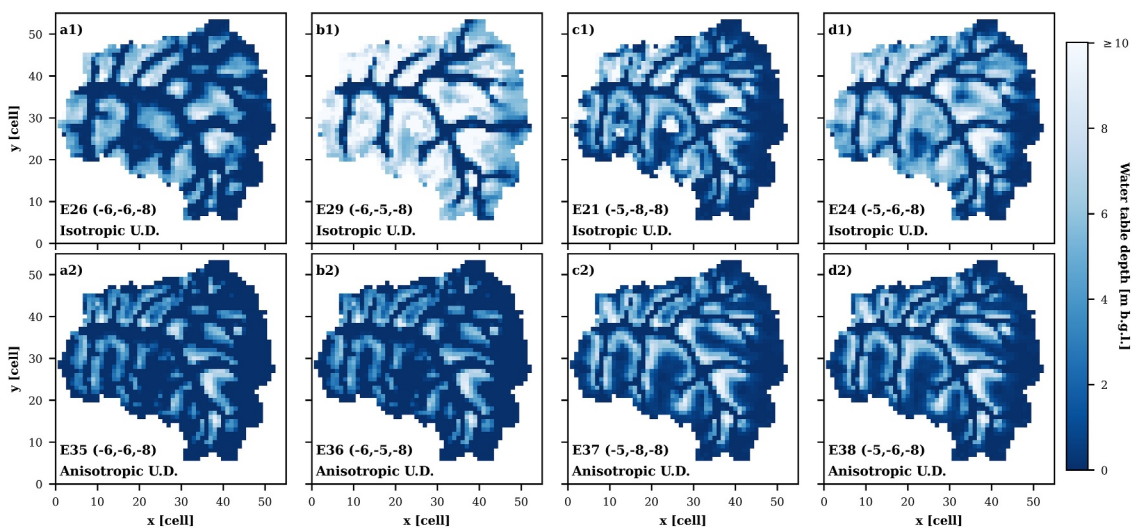

Figure 8. Simulated groundwater table distributions in winter for selected isotropic and anisotropic cases with $\phi^{U.D.} = 0.42$. Values in parenthesis show the log K_x [m/s] of the units U.D., weathered rock (W.R.) and Bedrock for each case. The units W.R. and Bedrock are isotropic for all models. For anisosotropic simulations, anisotropy is only included in U. D, with $K_x = K_y = 10K_z$. For description of the numerical experiments the reader is referred to Table 2.

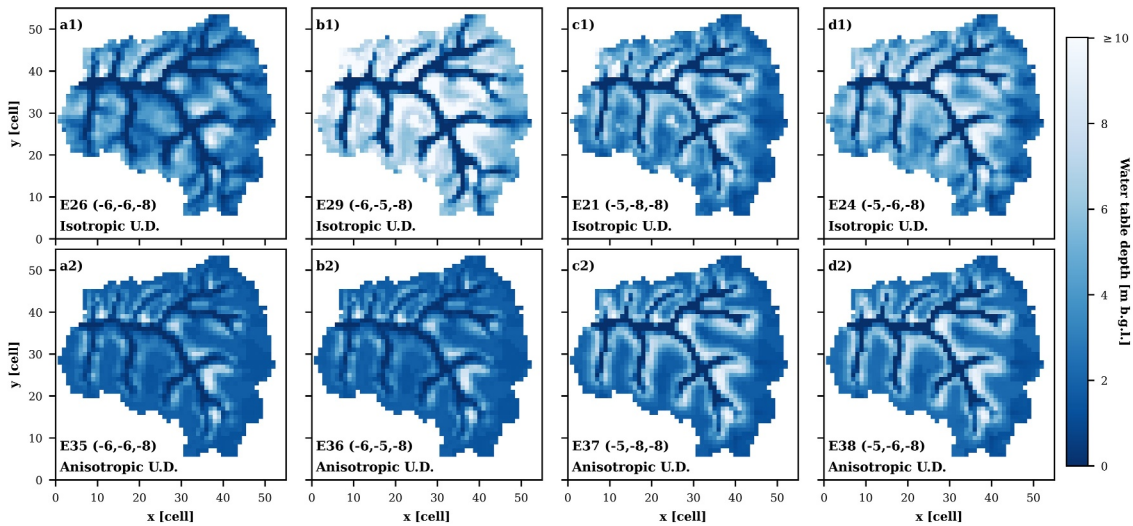

Figure 9. Simulated groundwater table distributions in summer for selected isotropic and anisotropic cases with $\phi^{U.D.} = 0.42$. Values in parenthesis show the log K_x [m/s] of the units U.D., weathered rock (W.R.) and Bedrock for each case. The units W.R. and Bedrock are isotropic for all models. For anisosotropic simulations, anisotropy is only included in U. D, with $K_x = K_y = 10K_z$. For description of the numerical experiments the reader is referred to Table 2.

space. For each set of tested van Genuchten parameters, we adopted two different approaches to relate the water content and the suction for S_{fc} and S_{wp}. First, we only varied α and n, keeping the same values of S_{fc} and S_{wp} as for Base Case I, with $S_{fc} = 0.53$ and $S_{wp} = 0.15$. Second, we also varied the values of S_{fc} and S_{wp} based on suctions of 3.3 and 150 m, respectively, according to the derived set of SWRCs (Figure 11).

Simulated soil water contents of the 12 models with different parameter combinations of α, n, S_{fc} and S_{wp} (Stage III in Table 2) are compared regarding the weighted average saturation of the uppermost 1 m relative to Base case I in winter and summer (Figures 12 and 13). A lower α (Figure 13a1) leads to higher soil water saturations, especially in areas where the U.D. are thinner, whereas a lower n (Figure 13c1) shows only mildly changes within the defined range. A simultaneous reduction of both parameters exhibits a combination of both effects (Figure 13e1). During winter and summer, lower values for both α and n generally result in higher soil moisture contents compared to the Base case I. In winter, these differences are very low due to the high saturation throughout the entire catchment, while they are considerably more significant in summer. At higher values of α and n (Figures 13b1, 13d1 and 13f1), a decrease in soil saturation is simulated, which is more pronounced in grassland areas. The observed impact of lower α and n yielding higher saturations, whereas higher values having

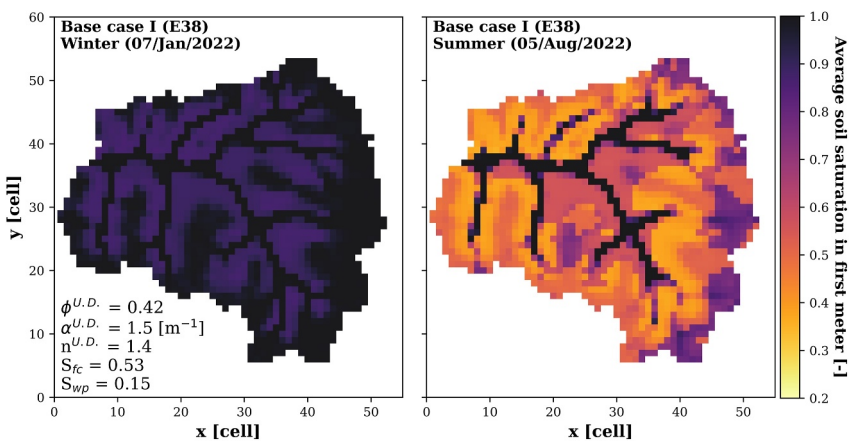

Figure 10. Simulated saturation in the first meter of soil for selected days representing winter and summer conditions for experiment Base case I (E38, Table 2.).

10.1029/2025WR040785

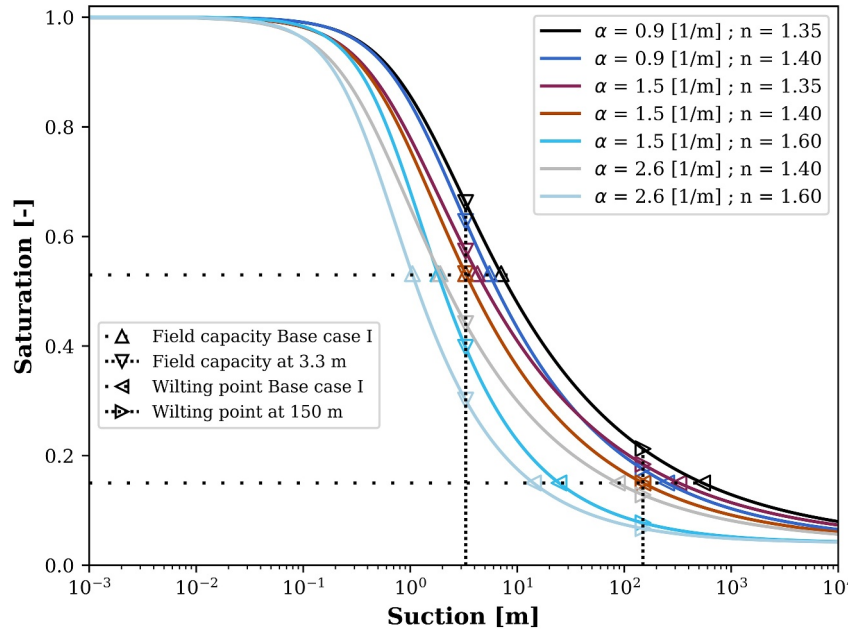

Figure 11. Different cases of van Genuchten parameters, field capacities and wilting points. Note that suction (matric potential) refers to a negative pressure head.

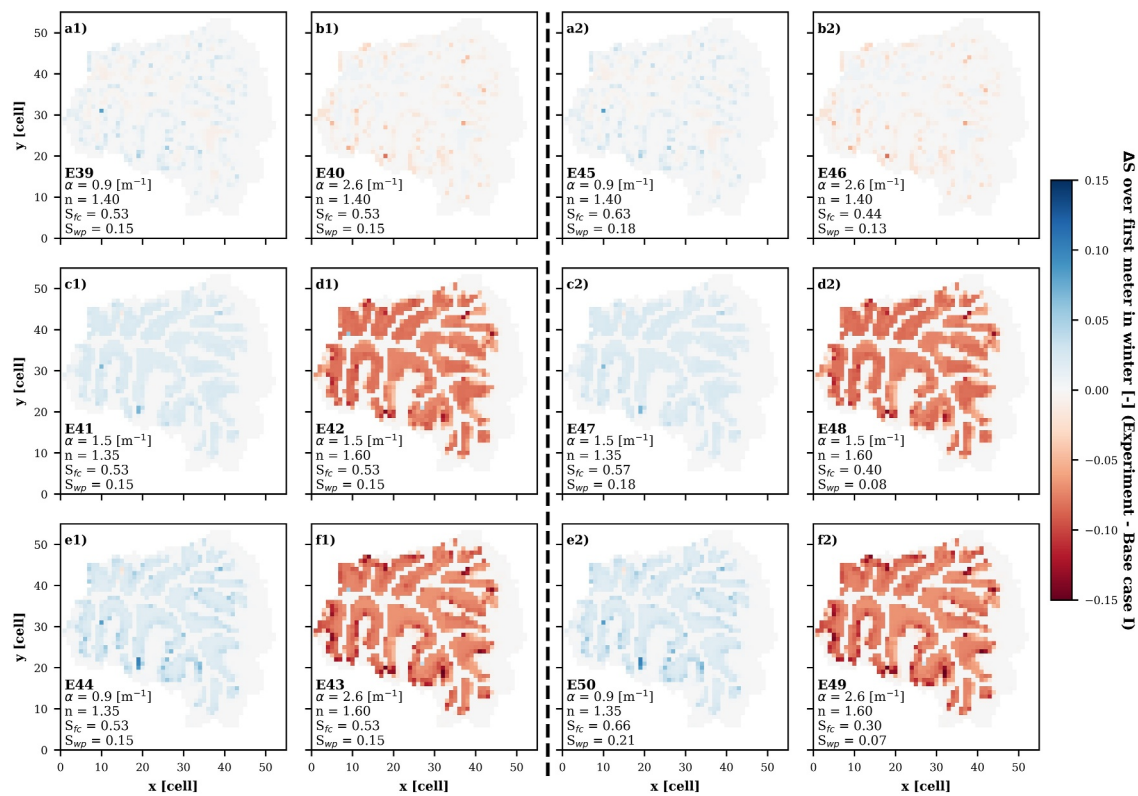

Figure 12. Comparison of average saturations in the first meter of soil in winter. The dashed line divides the cases considering the same S_{fc} and S_{wp} of the Base case I (left) and the ones varying those parameters according to the redefined soil water retention curves (right).

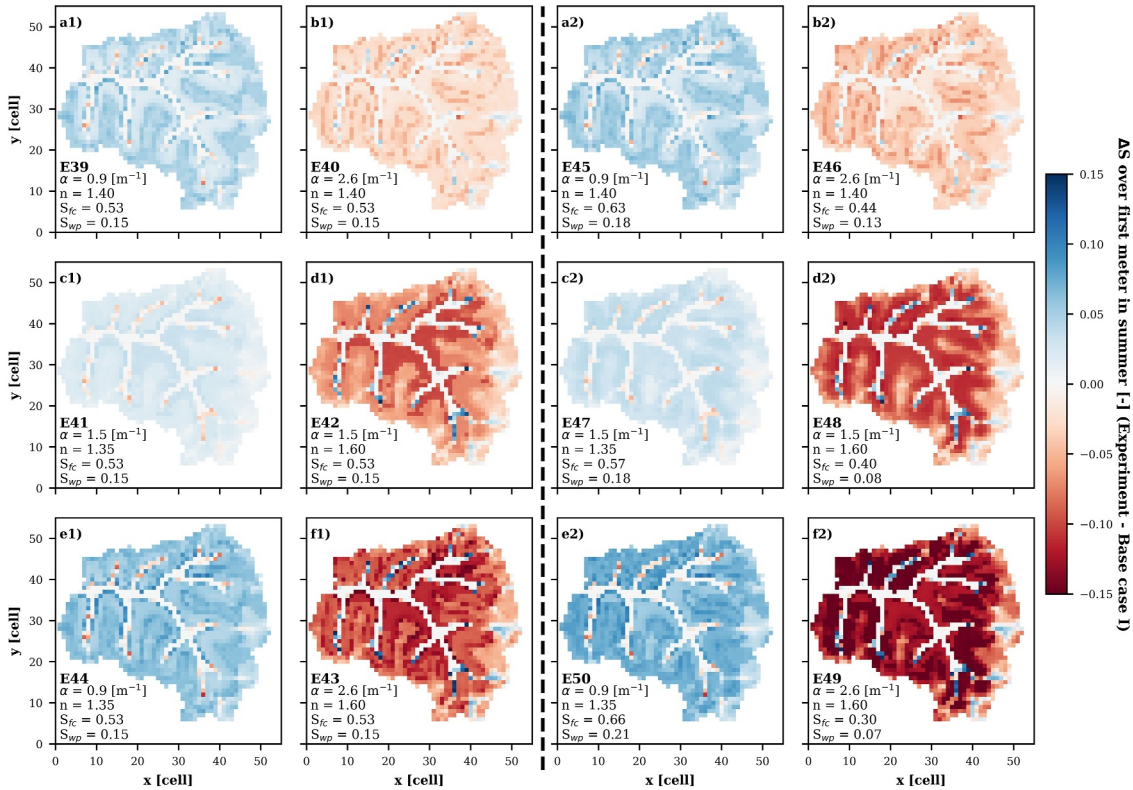

Figure 13. Comparison of average saturation in the first meter of soil in summer. The dashed line divides the cases considering the same S_{fc} and S_{wp} of the Base case I (left) and the ones varying those parameters according to the redefined soil water retention curves (right).

the opposite effect, agrees with what is suggested by the SWRCs presented in Figure 11, where the darker curves corresponding to lower α and n values determine higher saturations than the lighter curves at a given suction.

With regard to a change in S_{fc} and S_{wp} at constant α and n, virtually no differences can be detected during the winter (left vs. right panel in Figure 12), suggesting that these parameters are insensitive during wet conditions, which can be explained by evapotranspiration being typically energy-limited during winter in the region (Koster et al., 2024). In summer, however, when evapotranspiration is limited by the availability of water due to a lower SWC as well as the larger influence of root water uptake and the related stress response functions, changes in S_{fc} and S_{wp} have a significant impact on the simulations results in all cases (left vs. right panel in Figure 13). Overall, our results indicate a relevant influence of the unsaturated parameters α, n, S_{fc} and S_{wp} for IHMs, especially for simulations under water-limited conditions. This aligns with the limited previous studies that have indicated the importance of van Genuchten parameters (Rihani et al., 2010), and particularly S_{wp} (Srivastava et al., 2014) in the context of PF-CLM models.

To further explore the role of the S_{fc} and S_{wp}, we selected the model with the best statistical performance regarding river discharge (E44; with anisotropic $K^{U.D.}$, $\phi^{U.D.} = 0.42$, $n = 1.35$, $\alpha = 0.9$ [1/m], $S_{fc} = 0.53$ and $S_{wp} = 0.15$; NSE = 0.59 and KGE = 0.72). This model constitutes our Base case II. Since models with lower α and n showed better discharge performance, we ran additional experiments with smaller n and α values, outside of our previously defined parameter range. Interestingly, for $n < 1.35$ the simulations became numerically unstable. We attribute this to higher soil moisture that caused saturation excess conditions and thus increased overland flow, which forced very small time steps and led to prohibitively long computational times. We therefore retained the originally selected parameter range.

The two analyzed cases of S_{fc} and S_{wp} (E44 and E50 in Figure 13) for $n = 1.35$ and $\alpha = 0.9$ [1/m] behaved similarly with respect to river discharge despite different simulated soil saturations, highlighting the advantage to include SWC observations to constrain the space of possible solutions for IHMs. Therefore, with α and n fixed, we

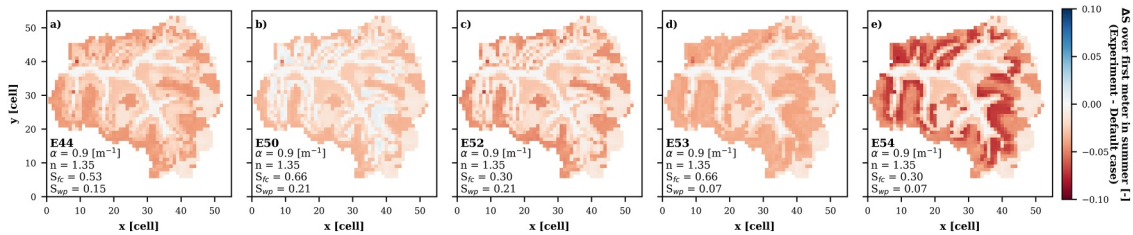

Figure 14. Effect of field capacity and wilting point during summer for models with fixed van Genuchten parameters. Default case (E51) uses $S_{fc} = 1.0$ and $S_{wp} = 0.1$. For description of the numerical experiments the reader is referred to Table 2.

run four further simulations with different combinations of S_{fc} and S_{wp}. One of these parameter combinations was $S_{fc} = 1.0$ and $S_{wp} = 0.1$, which are the default values defined in PF-CLM (experiment E51 in Table 2). Although these are not very realistic values, this case was defined as the new reference scenario for comparison (Default case, Figure 14), since the vast majority of PF-CLM studies (see Table S1 in Supporting Information S1) do not explicitly mention S_{fc} or S_{wp} as modified parameters, nor do they state that these parameters are linked to SWRCs, indicating that the default values were used. This lack of attention is also the reason why we have relaxed the assumption of linking S_{fc} and S_{wp} to the defined SWRCs.

Similar to the model variants with variable van Genuchten parameters (Figures 12 and 13), changes in S_{fc} and S_{wp} for a fixed set of α and n values have a negligible effect in shallow soil saturation during winter (Figure S12 in Supporting Information S1), but a significant impact during summer (Figure 14). Furthermore, all tested cases exhibited lower soil saturations compared to the Default case, that is, $\Delta S \leq 0$, which was more pronounced in the case with lower S_{fc} and S_{wp} (Figure 14e), particularly in forest areas (cf. Figure 2c). This is due to the fact that under water-limited conditions, lower S_{fc} and S_{wp} increase the root water uptake at a given saturation by reducing stomatal resistance (driven by a water-stress response function) and thereby increasing evapotranspiration (Ferguson et al., 2016). This also becomes apparent when comparing the temporal evolution of simulated soil saturations to our water content observations (Figure 15). This model parametrization (E54 in Table 2), giving the lowest soil moisture, was able to reproduce the time series of soil saturation in winter for both land uses, but not in summer, particularly for SWC sensors installed in grasslands, where the simulated saturation is higher than the observed one. Since all cases simulated with different S_{fc} and S_{wp} perform statistically the same as Base case II regarding stream discharge, we therefore consider this driest model in terms of shallow soil saturations as our Final model.

3.4. Streamflow Time Series and Manning's Roughness Scaling

The time series of observed and simulated discharge of the Final model are presented in Figure 16a. To explore how to further improve the model's statistical performance, we additionally applied a scaling of the Manning's roughness coefficient following the methodology of Foster (2018). For this purpose, we increased the Manning's coefficient by a factor of 50 for grassland cells and by a factor of 150 for forest cells that were not associated with stream segments. The latter were defined as cells in the top model layer with positive pressure on the day of lowest simulated discharge. Interestingly, in our case this scaling improved the NSE, but not the KGE (Figure 16a). This can be explained by an improved correlation component (r in Figure 16) and a deterioration in the relative variability component (a in Figure 16), which is part of the KGE. The bias error (b in Figure 16a) remained negligible for both model variants. These results again highlight the importance of evaluating IHMs using multiple statistical metrics and suggest that scaling approaches do not always improve statistical performance. Furthermore, Figure 16b shows that the impact of scaling Manning's coefficient does not necessarily correspond to events of high precipitation, but rather to sequences of events. This indicates that Manning's roughness could have a greater influence under sustained wet conditions, in contrast, for example, to S_{fc} and S_{wp}, which were found to be more relevant during dry periods, underscoring the inherent complexity of IHMs. In this context, it has to be noted that the scaling of Manning's coefficients is expected to have a more pronounced effect for higher temporal resolutions than analyzed in this work (1 hour), as discussed by Foster (2018).

10.1029/2025WR040785

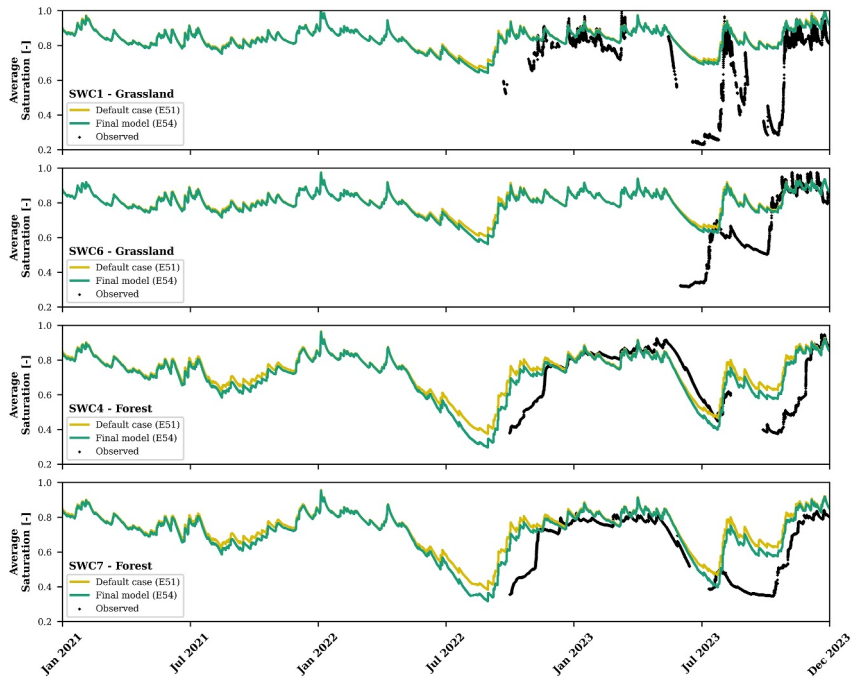

Figure 15. Observed and simulated average soil saturation in first meter for the Default case (E51, $S_{fc} = 1.0$ and $S_{wp} = 0.1$) and for the Final model (E54, $S_{fc} = 0.30$ and $S_{wp} = 0.07$). For description of the numerical experiments the reader is referred to Table 2.

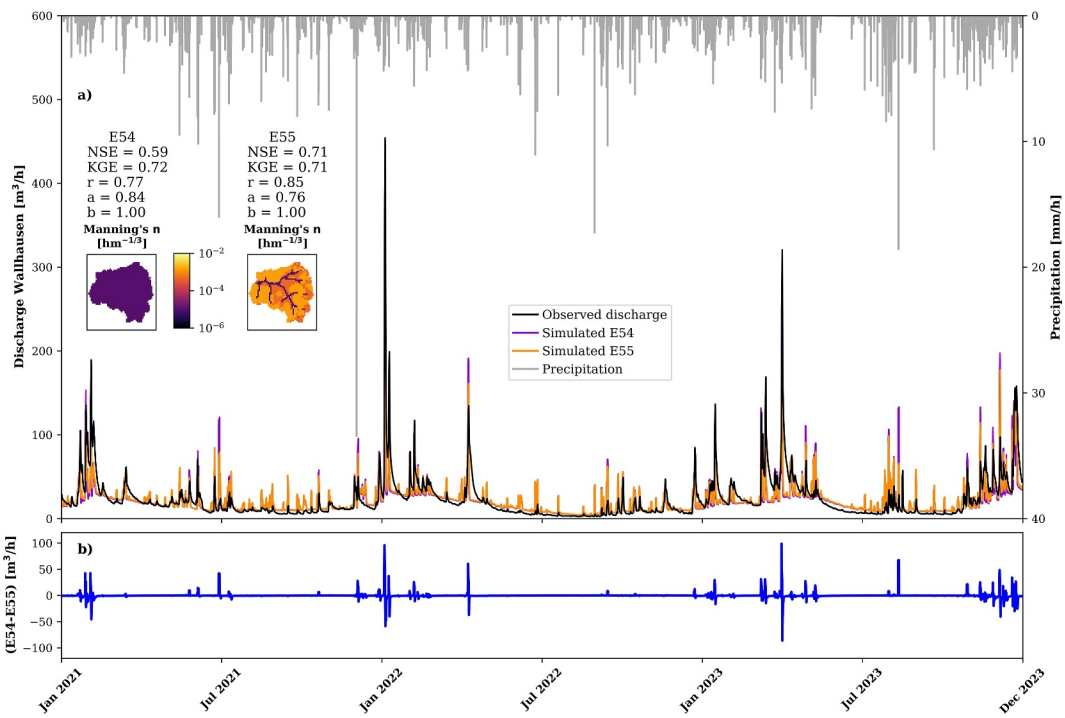

Figure 16. Simulated and observed discharge in Wallhausen at daily resolution for the Final model without and with scaled Manning's coefficients. r, a, and b represent the different components of the Kling-Gupta efficiency.

4. Concluding Remarks

In this work, we analyzed the effects of hydraulic conductivity conceptualization and parametrization, such as the layering of hydrogeological units and their anisotropy, the van Genuchten parameters α and n, as well as properties related to soil-vegetation interactions, namely field capacity and wilting point, in the context of integrated hydrologic modeling. To this end, we conducted a comprehensive sensitivity analysis intending to complement classical global or local approaches. One of our aims was to help modelers to identify and assess principal effects of subsurface conceptualization and parametrization in realistic domains characterized by physical heterogeneity, seasonality, and uncertainty in boundary conditions and geometry. For this purpose, we used hydrological observations to assess the plausibility of our numerical experiments, rather than a classical model calibration. In doing so, we had to make some assumptions and simplifications, for instance in the conceptualization of the hydrogeological units or the use of a meteorological forcing based on measurements outside of our study area. Nevertheless, based on the results of this work, we can draw the following conclusions:

- Selecting an appropriate temporal scale is one of the first considerations when evaluating an IHM. Here, both the distinguishability with regard to the objective function and the representation of nonlinear processes must be taken into account.
- Given their strong influence within the critical zone, the hydraulic properties of shallow geologic horizons should be routinely included in sensitivity analyses of IHMs.
- Simulations from isotropic K fields differ from those obtained with anisotropy, suggesting that anisotropy ratios should be incorporated into parameter optimization schemes.
- When anisotropy was incorporated, we could not isolate the hydraulic influence of the W.R. unit, which indicates non-uniqueness of the parameter combinations. Thus, constraining the space of possible solutions for an IHM requires complementary observations, such as streamflow, soil moisture, and groundwater levels. In this regard, statistical performance should be assessed with multiple metrics rather than a single one.
- Parameters that define the SWRC appears to be highly sensitive for IHMs.
- Transient simulations reveal seasonal differences in parameter sensitivity under water-limited versus energy-limited conditions.
- Field capacity (S_{fc}) and wilting point (S_{wp}), often not adjusted in IHM applications, can strongly influence simulated processes and should be tied to SWRCs or physically based definitions.
- Scaling of Manning's coefficients did not yield better results in our case and appears to be relevant only for larger catchments or higher temporal resolution.

Furthermore, as demonstrated throughout this work, the hydraulic properties of shallow soils and unconsolidated deposits exert a strong control on the hydrologic response of systems such as the one studied here, which are characterized by relatively thin sedimentary layers overlying rock formations in a temperate oceanic climate dominated by grasslands and forests. In the context of integrated hydrologic modeling, we therefore provide the following recommendations for parameter ranges representative of unconsolidated deposits with sandy loam to silty loam textures, which can serve as initial bounds for sensitivity analyses or inverse modeling frameworks aimed at constraining hydrologic simulations of similar systems:

- K typically ranges between 10^{-6} to 10^{-4} m/s.
- The effects of anisotropy of K should be tested, and a horizontal to vertical ratio of about 10 is recommended for exploratory simulations.
- Porosity commonly ranges between 0.40 and 0.50.
- Initial estimates of van Genuchten parameters may be derived from pedotransfer functions based on soil texture. In this study, α varied from 0.9 to 2.6 [1/m], and n from 1.3 to 1.6.
- After defining the SWRC, the S_{fc} and S_{wp} should be assigned based on physically meaningful suctions, typically 3.3 and 150 m, respectively.

We expect that the findings from our efficient sensitivity analysis approach will help modelers to understand the controls of hydraulic conductivity and unsaturated parameters in the critical zone, while addressing calibration challenges associated with high computational demands and model complexity. Nevertheless, achieving better model performance would likely require adjustment of additional vegetation-related parameters, such as leaf area index or aerodynamic roughness length. In this regard, even the formulation of the root water uptake, which was defined here in terms of water saturation instead of pressure, as in most studies using PF-CLM, could affect the simulated soil water contents. Beyond the analysis of the model parameters, our results show that considering

only one observed variable as a reference does not guarantee a unique solution. Thus, other observations in addition to streamflow, such as soil moisture and groundwater level distributions, are paramount for the evaluation of integrated hydrologic simulations and for a better understanding of the hydrological processes within the critical zone. Accurately representing the interactions between surface water and groundwater is crucial, as these exchanges sustain ecosystems, regulate water quality, and determine the availability of water resources. This study contributes toward that end by improving the representation of subsurface processes in IHMs through a sensitivity analysis that identifies realistic parameter ranges and highlights their influence on model performance.

Conflict of Interest

The authors declare no conflicts of interest relevant to this study.

Data Availability Statement

The files required to reproduce the results of the Final model version are archived and openly available via https://doi.org/10.5281/zenodo.17359813.

Acknowledgments
The authors thank to three reviewers for their constructive comments that certainly improved the quality and content of this work. Furthermore, we also thank the editor and the associate editor for their time and attention on the manuscript. This research has been funded by the Deutsche Forschungsgemeinschaft (DFG, Project Number: 459684982). Finally, the authors gratefully acknowledge the support of Selina Hillmann and Matthias Bockstiegel in geoelectrical surveys. Open Access funding enabled and organized by Projekt DEAL.

References

Assi, A. T., Blake, J., Mohtar, R. H., & Braudeau, E. (2019). Soil aggregates structure-based approach for quantifying the field capacity, permanent wilting point and available water capacity. *Irrigation Science*, *37*(4), 511–522. https://doi.org/10.1007/s00271-019-00630-w

Atchley, A. L., & Maxwell, R. M. (2011). Influences of subsurface heterogeneity and vegetation cover on soil moisture, surface temperature and evapotranspiration at hillslope scales. *Hydrogeology Journal*, *19*(2), 289–305. https://doi.org/10.1007/s10040-010-0690-1

Bakker, M., & Bot, B. (2024). The effective vertical anisotropy of layered aquifers. *Groundwater Series*, *63*(1), 68–75. https://doi.org/10.1111/gwat.13432

Bogena, H. R., Herbst, M., Huisman, J., Rosenbaum, U., Weuthen, A., & Vereecken, H. (2010). Potential of wireless sensor networks for measuring soil water content variability. *Vadose Zone Journal*, *9*(4), 1002–1013. https://doi.org/10.2136/vzj2009.0173

Bogena, H. R., Huisman, J. A., Baatz, R., Hendricks Franssen, H.-J., & Vereecken, H. (2013). Accuracy of the cosmic-ray soil water content probe in humid forest ecosystems: The worst case scenario: Cosmic-ray probe in humid forested ecosystems. *Water Resources Research*, *49*(9), 5778–5791. https://doi.org/10.1002/wrcr.20463

Bogena, H. R., Weuthen, A., & Huisman, J. A. (2022). Recent developments in wireless soil moisture sensing to support scientific research and agricultural management. *Sensors*, *22*(24), 9792. https://doi.org/10.3390/s22249792

Brooks, P. D., Chorover, J., Fan, Y., Godsey, S. E., Maxwell, R. M., McNamara, J. P., & Tague, C. (2015). Hydrological partitioning in the critical zone: Recent advances and opportunities for developing transferable understanding of water cycle dynamics: Critical zone hydrology. *Water Resources Research*, *51*(9), 6973–6987. https://doi.org/10.1002/2015wr017039

Carlotto, T., Klaus, J., & Chaffe, P. L. B. (2023). An open-source gis preprocessing tool for the parflow hydrological model (pfgis-tool v1.0.0). *Environmental Modelling & Software*, *169*, 105824. https://doi.org/10.1016/j.envsoft.2023.105824

Chiogna, G., Cirpka, O. A., & Herrera, P. A. (2015). Helical flow and transient solute dilution in porous media. *Transport in Porous Media*, *111*(3), 591–603. https://doi.org/10.1007/s11242-015-0613-7

Condon, L. E., Markovich, K. H., Kelleher, C. A., McDonnell, J. J., Ferguson, G., & McIntosh, J. C. (2020). Where is the bottom of a watershed? *Water Resources Research*, *56*(3), e2019WR026010. https://doi.org/10.1029/2019wr026010

Dörr, W., & Stein, E. (2019). Precambrian basement in the rheic suture zone of the central European variscides (odenwald). *International Journal of Earth Sciences*, *108*(6), 1937–1957. https://doi.org/10.1007/s00531-019-01741-7

DWD. (2024). Stündliche stationsmessungen wetterdaten. Deutscher wetterdienst (dwd) climate data center (Cdc).

Enemark, T., Peeters, L. J., Mallants, D., & Batelaan, O. (2019). Hydrogeological conceptual model building and testing: A review. *Journal of Hydrology*, *569*, 310–329. https://doi.org/10.1016/j.jhydrol.2018.12.007

Engdahl, N. B. (2024). Impacts of permeability uncertainty in a coupled surface-subsurface flow model under perturbed recharge scenarios. *Water Resources Research*, *60*(3), e2023WR035975. https://doi.org/10.1029/2023wr035975

Fang, Z., Bogena, H., Kollet, S., Koch, J., & Vereecken, H. (2015). Spatio-temporal validation of long-term 3d hydrological simulations of a forested catchment using empirical orthogonal functions and wavelet coherence analysis. *Journal of Hydrology*, *529*, 1754–1767. https://doi.org/10.1016/j.jhydrol.2015.08.011

Fang, Z., Bogena, H., Kollet, S., & Vereecken, H. (2016). Scale dependent parameterization of soil hydraulic conductivity in 3d simulation of hydrological processes in a forested headwater catchment. *Journal of Hydrology*, *536*, 365–375. https://doi.org/10.1016/j.jhydrol.2016.03.020

Ferguson, I. M., Jefferson, J. L., Maxwell, R. M., & Kollet, S. J. (2016). Effects of root water uptake formulation on simulated water and energy budgets at local and basin scales. *Environmental Earth Sciences*, *75*(4), 316. https://doi.org/10.1007/s12665-015-5041-z

Foster, M., & M. Maxwell, R. (2018). Sensitivity analysis of hydraulic conductivity and manning's n parameters lead to new method to scale effective hydraulic conductivity across model resolutions. *Hydrological Processes*, *33*(3), 332–349. https://doi.org/10.1002/hyp.13327

Gupta, H. V., Kling, H., Yilmaz, K. K., & Martinez, G. F. (2009). Decomposition of the mean squared error and nse performance criteria: Implications for improving hydrological modelling. *Journal of Hydrology*, *377*(1–2), 80–91. https://doi.org/10.1016/j.jhydrol.2009.08.003

Herzog, A., Hector, B., Cohard, J., Vouillamoz, J., Lawson, F. M. A., Peugeot, C., & de Graaf, I. (2021). A parametric sensitivity analysis for prioritizing regolith knowledge needs for modeling water transfers in the West African critical zone. *Vadose Zone Journal*, *20*(6), e20163. https://doi.org/10.1002/vzj2.20163

HLNUG. (2017). Hydrogeologie von hessen — odenwald und sprendlinger horst. Retrieved from https://www.hlnug.de/fileadmin/dokumente/wasser/hydrogeologie/Odenwaldbericht_2017_Web.pdf

HVBG. (2024a). *Digitale topographische karte 1:25 000 (dtk25)*. Hessische Verwaltung für Bodenmanagement und Geoinformation.

HVBG. (2024b). *Digitales geländemodell (dgm1)*. Hessische Verwaltung für Bodenmanagement und Geoinformation.

Ibrahimi, K., & Alghamdi, A. G. (2022). Available water capacity of sandy soils as affected by biochar application: A meta-analysis. *Catena*, *214*, 106281. https://doi.org/10.1016/j.catena.2022.106281

Jaros, A., Rossi, P. M., Ronkanen, A.-K., & Kløve, B. (2019). Parameterisation of an integrated groundwater-surface water model for hydrological analysis of boreal aapa mire wetlands. *Journal of Hydrology*, *575*, 175–191. https://doi.org/10.1016/j.jhydrol.2019.04.094

Jefferson, J. L., Gilbert, J. M., Constantine, P. G., & Maxwell, R. M. (2015). Active subspaces for sensitivity analysis and dimension reduction of an integrated hydrologic model. *Computers and Geosciences*, *83*, 127–138. https://doi.org/10.1016/j.cageo.2015.07.001

Koch, J., Cornelissen, T., Fang, Z., Bogena, H., Diekkrüger, B., Kollet, S., & Stisen, S. (2016). Inter-comparison of three distributed hydrological models with respect to seasonal variability of soil moisture patterns at a small forested catchment. *Journal of Hydrology*, *533*, 234–249. https://doi.org/10.1016/j.jhydrol.2015.12.002

Kollet, S. J. (2009). Influence of soil heterogeneity on evapotranspiration under shallow water table conditions: Transient, stochastic simulations. *Environmental Research Letters*, *4*(3), 035007. https://doi.org/10.1088/1748-9326/4/3/035007

Kollet, S. J., & Maxwell, R. M. (2006). Integrated surface–groundwater flow modeling: A free-surface overland flow boundary condition in a parallel groundwater flow model. *Advances in Water Resources*, *29*(7), 945–958. https://doi.org/10.1016/j.advwatres.2005.08.006

Koster, R. D., Feldman, A. F., Holmes, T. R. H., Anderson, M. C., Crow, W. T., & Hain, C. (2024). Estimating hydrological regimes from observational soil moisture, evapotranspiration, and air temperature data. *Journal of Hydrometeorology*, *25*(3), 495–513. https://doi.org/10.1175/jhm-d-23-0140.1

Kuffour, B. N. O., Engdahl, N. B., Woodward, C. S., Condon, L. E., Kollet, S., & Maxwell, R. M. (2020). Simulating coupled surface–subsurface flows with parflow v3.5.0: Capabilities, applications, and ongoing development of an open-source, massively parallel, integrated hydrologic model. *Geoscientific Model Development*, *13*(3), 1373–1397. https://doi.org/10.5194/gmd-13-1373-2020

Lachassagne, P., Dewandel, B., & Wyns, R. (2021). Review: Hydrogeology of weathered crystalline/hard-rock Aquifers—Guidelines for the operational survey and management of their groundwater resources. *Hydrogeology Journal*, *29*(8), 2561–2594. https://doi.org/10.1007/s10040-021-02339-7

Leonarduzzi, E., Maxwell, R. M., Mirus, B. B., & Molnar, P. (2021). Numerical analysis of the effect of subgrid variability in a physically based hydrological model on runoff, soil moisture, and slope stability. *Water Resources Research*, *57*(4), e2020WR027326. https://doi.org/10.1029/2020wr027326

Lu, Z., Wei, J., & Yang, X. (2024). Effects of hydraulic conductivity on simulating groundwater–land surface interactions over a typical endorheic river basin. *Journal of Hydrology*, *638*, 131542. https://doi.org/10.1016/j.jhydrol.2024.131542

Maples, S. R., Foglia, L., Fogg, G. E., & Maxwell, R. M. (2020). Sensitivity of hydrologic and geologic parameters on recharge processes in a highly heterogeneous, semi-confined aquifer system. *Hydrology and Earth System Sciences*, *24*(5), 2437–2456. https://doi.org/10.5194/hess-24-2437-2020

Maxwell, R. M. (2013). A terrain-following grid transform and preconditioner for parallel, large-scale, integrated hydrologic modeling. *Advances in Water Resources*, *53*, 109–117. https://doi.org/10.1016/j.advwatres.2012.10.001

Maxwell, R. M., Putti, M., Meyerhoff, S., Delfs, J., Ferguson, I. M., Ivanov, V., et al. (2014). Surface-subsurface model intercomparison: A first set of benchmark results to diagnose integrated hydrology and feedbacks. *Water Resources Research*, *50*(2), 1531–1549. https://doi.org/10.1002/2013wr013725

Niedda, M. (2004). Upscaling hydraulic conductivity by means of entropy of terrain curvature representation. *Water Resources Research*, *40*(4), W04206. https://doi.org/10.1029/2003wr002721

Peel, M. C., Finlayson, B. L., & McMahon, T. A. (2007). Updated world map of the köppen-geiger climate classification. *Hydrology and Earth System Sciences*, *11*(5), 1633–1644. https://doi.org/10.5194/hess-11-1633-2007

Rapp, G. A., Condon, L. E., & Markovich, K. H. (2020). Sensitivity of simulated Mountain block hydrology to subsurface conceptualization. *Water Resources Research*, *56*(10), e2020WR027714. https://doi.org/10.1029/2020wr027714

Rihani, J. F., Maxwell, R. M., & Chow, F. K. (2010). Coupling groundwater and land surface processes: Idealized simulations to identify effects of terrain and subsurface heterogeneity on land surface energy fluxes. *Water Resources Research*, *46*(12), W12523. https://doi.org/10.1029/2010wr009111

Rojas, R., Feyen, L., & Dassargues, A. (2008). Conceptual model uncertainty in groundwater modeling: Combining generalized likelihood uncertainty estimation and Bayesian model averaging. *Water Resources Research*, *44*(12), W12418. https://doi.org/10.1029/2008wr006908

Sanchez-Vila, X., Guadagnini, A., & Carrera, J. (2006). Representative hydraulic conductivities in saturated groundwater flow. *Reviews of Geophysics*, *44*(3), RG3002. https://doi.org/10.1029/2005rg000169

Schalge, B., Haefliger, V., Kollet, S., & Simmer, C. (2019). Improvement of surface run-off in the hydrological model parflow by a scale-consistent river parameterization. *Hydrological Processes*, *33*(14), 2006–2019. https://doi.org/10.1002/hyp.13448

Schulz, S., Siebert, C., Rödiger, T., Al-Raggad, M. M., & Merz, R. (2013). Application of the water balance model j2000 to estimate groundwater recharge in a semi-arid environment: A case study in the Zarqa river catchment, nw-jordan. *Environmental Earth Sciences*, *69*(2), 605–615. https://doi.org/10.1007/s12665-013-2342-y

Schulz, S., Walther, M., Michelsen, N., Rausch, R., Dirks, H., Al-Saud, M., et al. (2017). Improving large-scale groundwater models by considering fossil gradients. *Advances in Water Resources*, *103*, 32–43. https://doi.org/10.1016/j.advwatres.2017.02.010

Seck, A., Welty, C., & Maxwell, R. M. (2015). Spin-up behavior and effects of initial conditions for an integrated hydrologic model. *Water Resources Research*, *51*(4), 2188–2210. https://doi.org/10.1002/2014wr016371

Seifert, D., Sonnenborg, T. O., Refsgaard, J. C., Højberg, A. L., & Troldborg, L. (2012). Assessment of hydrological model predictive ability given multiple conceptual geological models. *Water Resources Research*, *48*(6), W06503. https://doi.org/10.1029/2011wr011149

Shepley, M. G. (2024). Vertical hydraulic conductivity and layered heterogeneity: From measurements to models. *Hydrogeology Journal*, *32*(4), 1017–1042. https://doi.org/10.1007/s10040-024-02773-3

Soltani, S. S., Fahs, M., Bitar, A. A., & Ataie-Ashtiani, B. (2022). Improvement of soil moisture and groundwater level estimations using a scale-consistent river parameterization for the coupled parflow-clm hydrological model: A case study of the upper rhine basin. *Journal of Hydrology*, *610*, 127991. https://doi.org/10.1016/j.jhydrol.2022.127991

Srivastava, V., Graham, W., Muñoz-Carpena, R., & Maxwell, R. M. (2014). Insights on geologic and vegetative controls over hydrologic behavior of a large complex basin – Global sensitivity analysis of an integrated parallel hydrologic model. *Journal of Hydrology*, *519*, 2238–2257. https://doi.org/10.1016/j.jhydrol.2014.10.020

Stein, E. (2001). The geology of the odenwald crystalline complex. *Mineralogy and Petrology*, *72*(1–3), 7–28. https://doi.org/10.1007/s007100170024

van Genuchten, M. T. (1980). A closed-form equation for predicting the hydraulic conductivity of unsaturated soils. *Soil Science Society of America Journal*, *44*(5), 892–898. https://doi.org/10.2136/sssaj1980.03615995004400050002x

Vereecken, H., Huisman, J., Pachepsky, Y., Montzka, C., van der Kruk, J., Bogena, H., et al. (2014). On the spatio-temporal dynamics of soil moisture at the field scale. *Journal of Hydrology*, *516*, 76–96. https://doi.org/10.1016/j.jhydrol.2013.11.061

Vereecken, H., Weynants, M., Javaux, M., Pachepsky, Y., Schaap, M. G., & van Genuchten, M. (2010). Using pedotransfer functions to estimate the Van genuchten–mualem soil hydraulic properties: A review. *Vadose Zone Journal*, *9*(4), 795–820. https://doi.org/10.2136/vzj2010.0045

Zhang, Y., & Schaap, M. G. (2017). Weighted recalibration of the rosetta pedotransfer model with improved estimates of hydraulic parameter distributions and summary statistics (rosetta3). *Journal of Hydrology*, *547*, 39–53. https://doi.org/10.1016/j.jhydrol.2017.01.004